Electronic Supplementary Material (ESI) for Sustainable Energy & Fuels.

SUPPORTING INFORMATION

N-Annulated Perylene Diimide Dimers: The Effect of Thiophene Bridges on Physical, Electronic, Optical, and Photovoltaic Properties

Arthur D. Hendsbee, Sergey V. Dayneko, Jefferson A. Pells, Jonathan R. Cann, Gregory C. Welch*

Department of Chemistry
University of Calgary, 731 Campus Place NW
Calgary, Alberta, Canada T2N 1N4
gregory.welch@ucalgary.ca

Table of Contents:

Materials and Methods:

General synthetic details: All reactions were performed on bench top conditions or under oxygen free, dry, nitrogen atmosphere where indicated. All reactions that were heated conventionally were submerged in labarmor® bead bath and heated on a hotplate at the designated temperature. All microwave assisted syntheses were performed using a biotage® initiator and microwave reactor. The operational range for this instrument is 0-400W using a 2.45 GHz magnetron.

Materials: All materials and solvents were purchased from Sigma-Aldrich. Compound **(1)** and **(tPDI$_2$-hex)** were synthesized as reported.[1]

Nuclear Magnetic Resonance (NMR): Reported ^{1}H NMR and ^{13}C NMR spectra were acquired on either Bruker Ascend 500 mHz, Avance 400 mHz, or DMX 300 mHz spectrometers at 300 K. All values are reported in parts per million (ppm) with the external reference $SiMe_4$. All experiments were performed with deuterated chloroform ($CDCl_3$). Multiplicities are reported as: Singlet (s), doublet (d), triplet and multiplet (m).

Mass Spectrometry (MS): Low-resolution MALDI mass spectrometry measurements were performed courtesy of Jian Jun (Johnson) Li in the Chemical Instrumentation Facility at the University of Calgary. A Bruker Autoflex III Smartbeam MALDI-TOF (Na:YAG laser, 355nm), setting in positive reflective mode, was used to acquire spectra. Operation settings were all typical, e.g. laser offset 62-69; laser frequency 200Hz; and number of shots 300. The target used was Bruker MTP 384 ground steel plate target. Sample solution (~ 1 µg/ml in dichloromethane) was mixed with matrix trans-2-[3-(4-tert-Butylphenyl)-2-methyl-2-propenylidene]malononitrile (DCTB) solution (~5 mg/ml in methanol). Pipetted 1µl solution above to target spot and dried in the fume hood.

Cyclic Voltammetry (CV): All cyclic voltammetry data was collected using a CH instruments potentiostat in a standard three electrode configuration equipped with a silver wire pseudo-reference, platinum wire counter electrode and glassy carbon working electrode. All CV experiments were performed in anhydrous dichloromethane (CH_2Cl_2) with ~0.1 M tetrabutylammonium hexafluorophosphate ($TBAPF_6$) supporting electrolyte. A dry N_2 purge to deoxygenate the solution was performed before scanning each sample at 100 mV/s. Solution CV measurements were carried out with a sample concentration of ~0.5 mg/mL in CH_2Cl_2. Ferrocene was used as an internal standard. Estimations of the ionization potentials (IP) and electron affinities (EA) were obtained by correlating the onset of oxidation and reduction, respectively, referenced to the Fc/Fc+ redox couple, to ferrocene assuming a conversion value of 4.8.

(IP) = (E_{ox}+4.8), (EA) = (E_{red}+4.8)

Optical Absorption Spectroscopy (UV-vis): All measurements were obtained using an Agilent Technologies Cary 60 UV-vis spectrometer at ~298K. All solution UV-vis experiments were run in chloroform ($CHCl_3$) using 2 mm quartz cuvettes and diluted to 1 % wt/v solutions, Thin-films were prepared by spin-coating 1 % wt/v solutions from $CHCl_3$ onto Corning glass micros slides at 2500 rpm. Prior to measurements, glass slides were cleaned with soap and water, acetone and isopropanol, followed by UV/ozone treatment using a Novascan UV/ozone cleaning system.

Photoluminescence Spectroscopy:

All measurements were obtained using an Agilent technologies Cary Eclipse Fluorescence Spectrophotometer at ~298K. All solution experiments were run in chloroform ($CHCl_3$) using 2 mm quartz cuvettes. Solutions were prepared by taking 20 µL of a 10 mg/mL solution and diluting to a total volume of 20 mL.

Polarized Optical Microscopy:

Polarized optical microscopy experiments were performed using an Olympus Bx53 microscope. Drop cast solutions were prepared from 1% wt/v solutions in $CHCl_3$.

Density Functional Theory: Calculations were carried out using Gaussian09,[2] input files and results were visualized using GausView05.[3] All alkyl chains were replaced with a methyl group. The B3LYP[4–6] level of theory with 6-31G(d,p)[7–12] basis set were used for the calculations. TD-SCF[13] calculations were performed from the optimized geometries. Single point calculations were performed on optimized structures in order to generate molecular orbitals.

Melting Point Determination: The melting or decomposition points were determined using a Stuart SMP40 apparatus operating from 50 to 400 ^oC with a ramp rate of 20 ^oC/min.

Solar Cell Fabrication: Devices were fabricated using ITO-coated glass substrates cleaned by sequential ultrasonic cleaning using detergent and deionized water, acetone and isopropanol followed by exposure to UV/ozone for 30 minutes. ZnO was deposited as a sol-gel precursor solution in air following the method of Sun *et al.*[14] The room temperature solution was filtered and spin-cast at a speed of 4000 rpm and then annealed at 200 °C in air for 1 hour. Active layer solutions were cast from 10 mg/ml solution in chloroform at 1500 rpm in air. All solutions were stirred overnight at room temperature prior to filtration through a PTFE filter. The substrates were then allowed to sit overnight before depositing the top contacts. Top contacts of MoO_x (10 nm) followed by 100 nm of silver were thermally deposited under vacuum at approximately $4*10^{-6}$ torr. The active areas of resulting devices were 0.09 cm^2. Completed devices were then tested in air using a Newport 92251A-1000 AM 1.5 solar simulator which had been calibrated using a standard silicon solar cell (Newport 91150V) to obtain an irradiance level of 1000 W/m^2.

Solar cell characterization: The current density-voltage (J-V) curves were measured by a Keithley 2420 source measure unit. The photocurrent was measured under AM 1.5 illumination at 1000 W/m^2 under a Solar Simulator (Newport 92251A-1000). The standard silicon solar cell (Newport 91150V) was used to calibrate light intensity. EQE was measured in a QEX7 Solar Cell Spectral Response/QE/IPCE Measurement System (PV Measurement, Model QEX7, USA) with an optical lens to focus the light into an area about 0.04 cm^2, smaller than the dot cell (0.09 cm^2). The silicon photodiode was used for the calibration of the EQE measurement system in the wavelength range from 300 to 1000 nm.

AFM: Atomic Force Microscope (AFM) measurements were performed by using either an Agilent Technologies 5500 Scanning Probe Microscope in contact mode or an AFM Workshop TT2-AFM in the tapping mode. A NanoInk PEN-0054-00 probe was

used for contact mode measurements and an AFM Workshop ACLA-10-W probe was used for tapping mode measurements. Thin film samples for AFM measurement were deposited on ITO/ZnO substrates following the same procedures as used for OPV device fabrication.

Thin-Film X-ray Diffraction: All X-ray diffraction experiments were performed on a PROTO AXRD Benchtop Powder Diffractometer using θ-2θ scans and Cu K-α radiation. Scans were performed from 2 degrees (2θ) to 30 degrees (2θ) while using a 2 mm divergence slit.

Synthetic procedures:

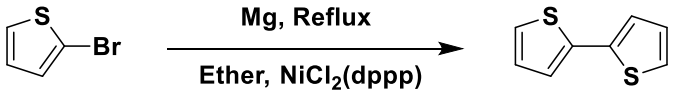

Synthesis of 2,2'-bithiophene (3): The synthesis of **(3)** followed literature conditions and spectroscopic data matched those previously reported.[15]

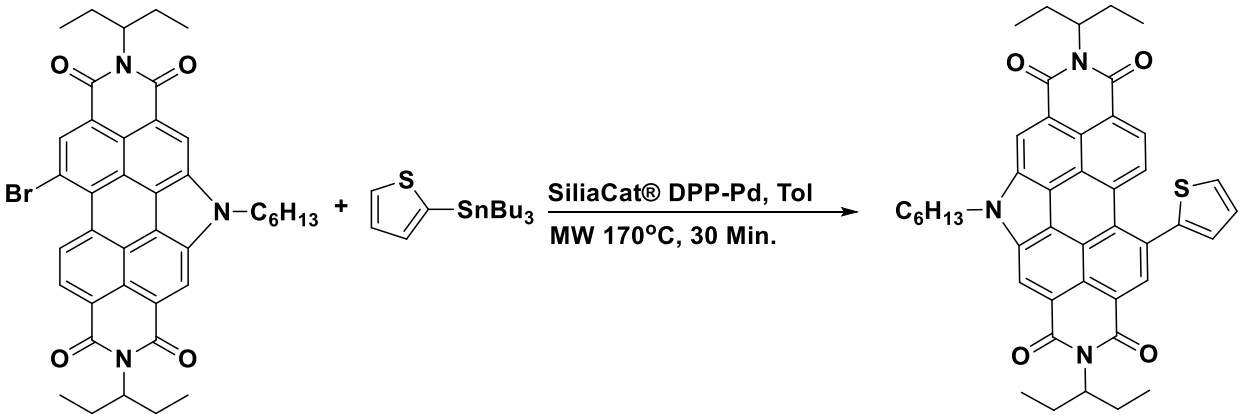

Synthesis of N-Hex-CAG-PDI-Thiophene (2): Br-EP-N-Hex-CAG-PDI (**(1)**, 1 g, 1.41 mmol) and SiliaCat® DPP-Pd (0.280 g, 0.25 mmol/g, 5 mol%) were combined in a microwave vial (10-20 mL) with a stir bar. 13 mL of toluene was added as the solvent and the reaction vial was then sealed with a Teflon® cap and purged with N_2 for 5 minutes. Next, 2-tributylstanyl thiophene (0.5 mL, 0.581 g, 1.56 mmol, 1.1 equiv.) was added to the sealed vial via syringe. Using a Biotage® Initiator microwave reactor, the reaction mixture was heated to 170 °C for 30 minutes with stirring, at which point TLC showed complete conversion of starting materials. The reaction was then diluted in 100 mL of DCM and slurried with 15 mL SiO_2 and 15 mL K_2CO_3 for 1 hour to remove tin containing by products. The mixture was then poured through a short silica plug and the solvent removed under reduced pressure to give a crude solid. The crude solid was recrystallized from ethanol (~50 mL) and filtered with Buchner funnel to afford an orange crystalline

solid, **N-Hex-CAG-PDI-Thiophene** (**(2)**, 0. 9 g, 1.3 mmol, 90 %) **^{1}H NMR (Chloroform-d, TMS/ppm) δ**: 9.06 (s, 1H), 9.02 (s, 1H) 8.81 (s, 1H), 8.51 (d, 1H, $J^3_{H\text{-}H}$= 9 Hz), 8.04 (d, 1H, $^3J_{H\text{-}H}$= 7 Hz), 7.70(d, 1H, $^3J_{H\text{-}H}$= 3 Hz), 7.34 (m, 2H), 5.21 (m, 2H), 4.91 (m,2H), 2.35 (m, 6H), 2.28 (m, 4H), 1.38 (m, 6H), 1.27 (m, 15 H)

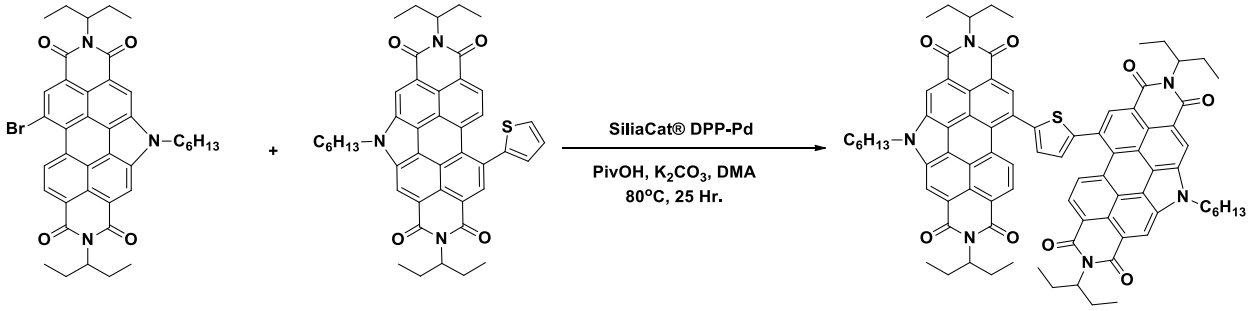

1 **2** **M1**

Synthesis of PDI-Th-PDI (M1): Br-EP-N-Hex-CAG-PDI (**(1)**, 0.601 g, 0.85 mmol, 1 equiv.), PDI-thiophene (**(2)**, 0.603 g, 0.85 mmol, 1 equiv.), pivalic acid (0.008 g, 0.078 mmol, 9 mol%), potassium carbonate (0.234 g, 1.7 mmol, 2 equiv.), and SiliaCat® DPP-Pd (0.168 g, 0.25 mmol/g, 5 mol %) were combined in a 10-20mL microwave vial with a stir bar. The reaction vial was then sealed with a Teflon® cap and purged with N_2 for 5 minutes. Dry, degassed DMA (~10 mL) was added to the sealed reaction vessel using a cannula. Once all the solvent was added, the vial was once again purged with N_2 for 5 minutes. The microwave vial was then placed into a labarmor® bead bath at 80 ^{o}C for 25 hours with stirring. After completion, the reaction mixture was cooled to room temperature and passed through a short silica plug using 100% DCM as the eluent. The collected solvent was then removed under reduced pressure to give a crude solid which was slurried in methanol for 20 minutes and collected via filtration. After collection, the crude solid was redissolved in DCM and wet loaded onto a normal phase silica column. A Hexane:DCM gradient was used to elute the product, with the product eluting at 100% DCM. The solvent was removed from the product fraction under reduced pressure. The remaining black, crystalline, solid was then recrystallized from hot isopropanol, cooled and collected by filtration to afford **PDI-Th-PDI** (**(M1)**, 0.796 g, 0.596 mmol, 70%). **^{1}H NMR (Chloroform-d, TMS/ppm) δ**: 9.04-9.10 (m, 6H), 8.77 (m, 4H), 7.69 (s, 2H), 5.18-5.25 (m, 4H), 4.94 (t, 4H, $^3J_{H\text{-}H}$= 7Hz), 2.34-2.36 (m, 12H), 2.01 (m, 8H), 1.46-1.51 (m, 12H), 0.83-0.88 (m,30H). **^{13}C NMR (Chloroform-d, TMS/ppm) δ**: 144.43, 134.47, 134.39, 127.40 124.34, 124.27, 122.53, 119.24, 46.40, 30.99, 30.83, 26.35, 24.65, 21.93, 13.41, 10.87. **LRMS (MALDI).** m/z exp: 1335.67 obtained: 1334.59 **Melting Point: M1** was stable up to 400 ^{o}C

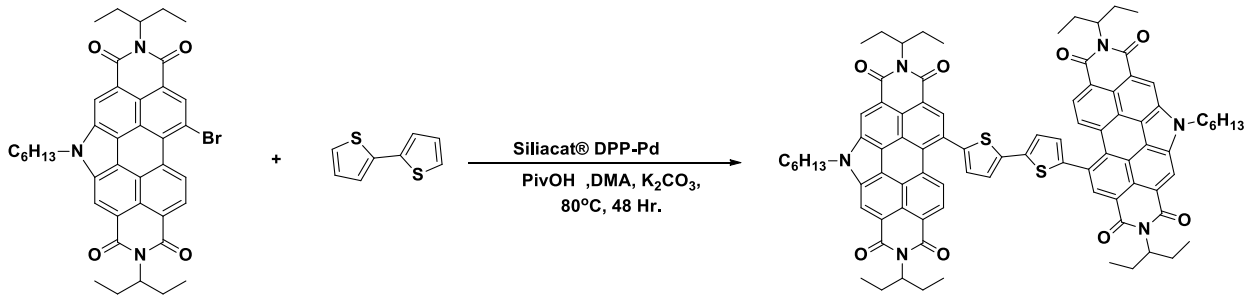

1 M2

Synthesis of PDI-Th-Th-PDI (M2): Br-EP-N-Hex-CAG-PDI (**(1)**, 0.227 g, 0.32 mmol, 2 equiv.), (**3**) Bithiophene (0.027 g, 0.16 mmol, 1 equiv.), PivOH (0.006 g, 0.059 mmol, 37 mol%), potassium carbonate (0.045 g, 0.32 mmol, 2 equiv.), and SiliaCat® DPP-Pd (0.033 g, 0.25 mmol/g, 5 mol%) were combined in a 2-5 mL microwave vial with stir bar. The reaction vial was then sealed with a Teflon® cap and purged with N_2 for 5 minutes. Dry, degassed DMA (~5 mL) was added to the sealed reaction vessel using a cannula. Once all the solvent was added, the vial was once again purged with N_2 for 5 minutes. The microwave vial was transferred to a labarmor® bead bath heated to 80 ^oC for 48 hours. After completion, the reaction mixture was cooled to room temperature and passed through a short silica plug using 100% DCM as the eluent. The collected solvent was then removed under reduced pressure to give a crude solid which was slurried in methanol for 20 minutes and collected via filtration. The crude solid was redissolved in DCM and wet loaded onto a normal phase silica column. The crude product was then purified by a Hexane:DCM gradient, with product eluting at 100% DCM. The solvent was removed from the product fraction under reduced pressure to give a black solid which was then slurried in methanol and collected by filtration to afford a black, crystalline, solid **PDI-Th-Th-PDI** (**(M2)**, 0.116 g, 0.082 mmol, 51.14%). **^{1}H NMR (Chloroform-d, TMS/ppm) δ**: 9.06 (s, 2H), 9.03 (s, 2H), 8.89 (s, 2H), 8.70 (d, 2H, $^3J_{H-H}$= 8 Hz), 8.58 (d, 2H, $^3J_{H-H}$= 8 Hz), 7.56 (d, 2H, $^3J_{H-H}$= 4 Hz), 7.38 (d, 2H, $^3J_{H-H}$= 3 Hz), 5.12-5.28 (m, 4H), 4.92 (t, 4H, $^3J_{H-H}$= 6 Hz), 2.19-2.36 (m, 12H), 1.92-2.03 (m, 8H), 1.25-1.47 (m, 12H), 0.83-1.00 (m, 30H). **13C NMR (Chloroform-d, TMS/ppm) δ**: 141.20, 138.64, 134.40, 134.29, 133.19, 132.46, 127.58, 127.51, 124.96, 124.21, 124.09, 122.47, 122.40, 119.26, 119.21,52.27, 46.36, 30.96, 30.81, 26.33, 24.63, 21.92, 13.40, 10.88, 10.85. **LRMS (MALDI).** m/z exp: 1417.79 obtained: 1416.58 **Melting Point: M2** was stable up to 400 ^oC.

NMR Spectra:

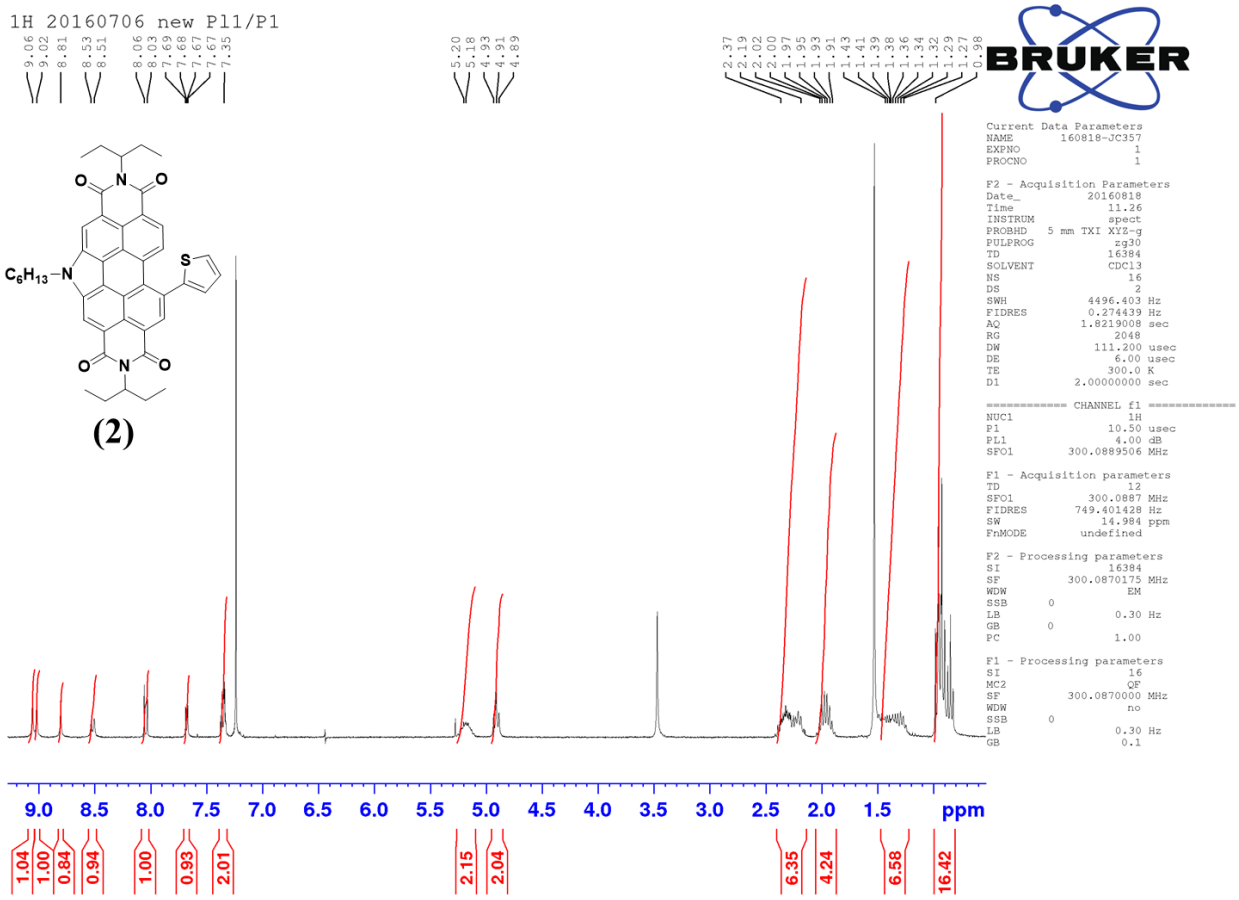

Figure S1: ^{1}H NMR spectra of compound **(2)**.

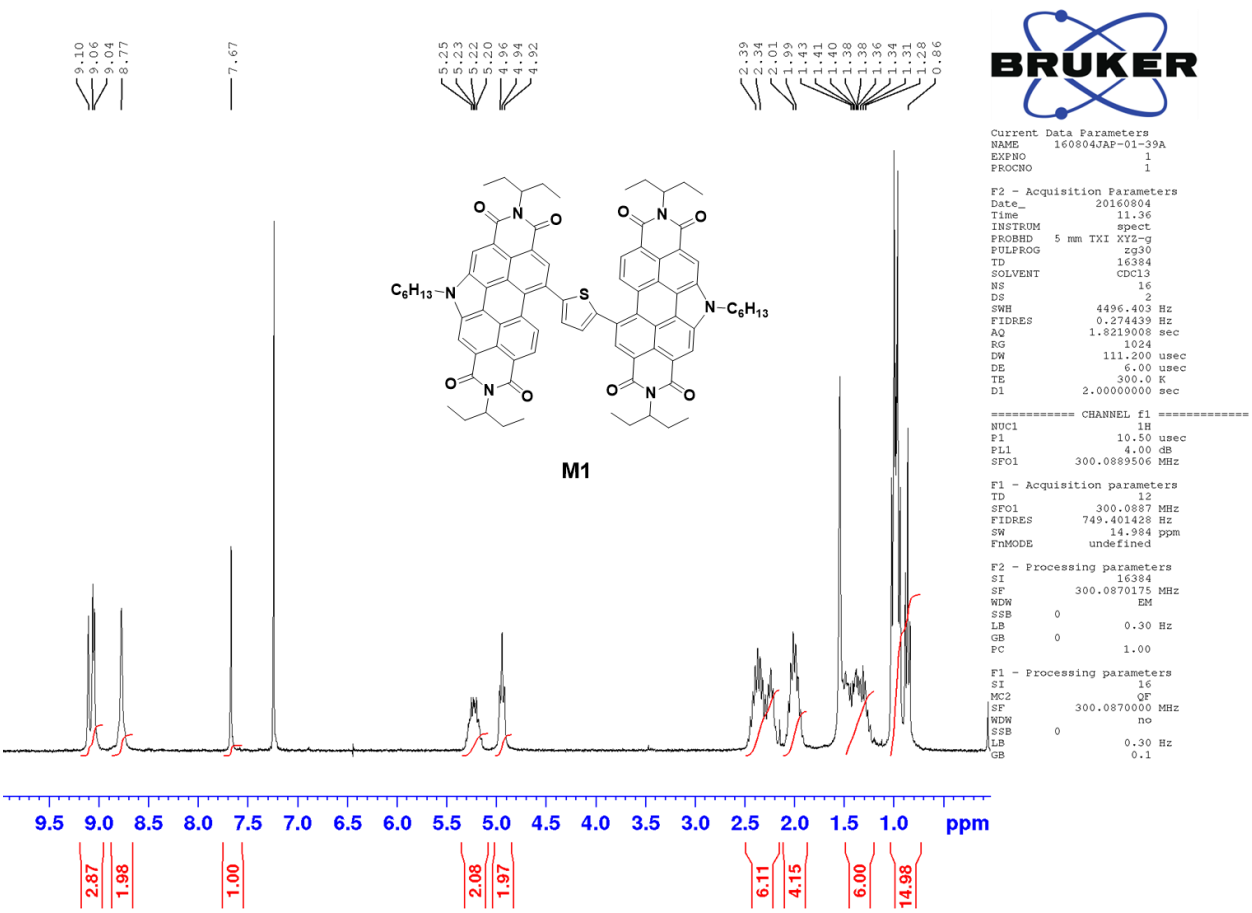

Figure S2: ^{1}H NMR spectrum of **M1**.

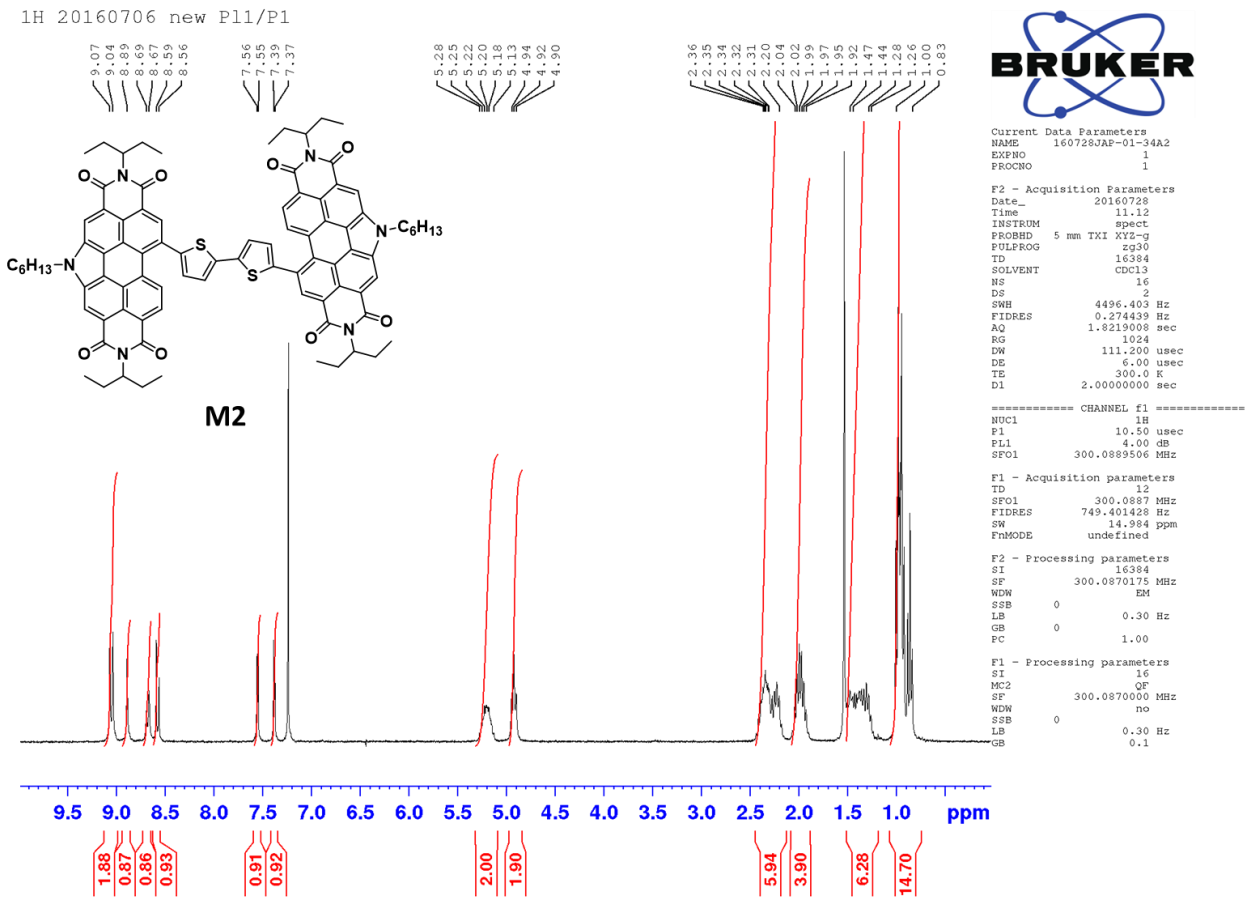

Figure S3: ^{1}H NMR spectrum of **M2**.

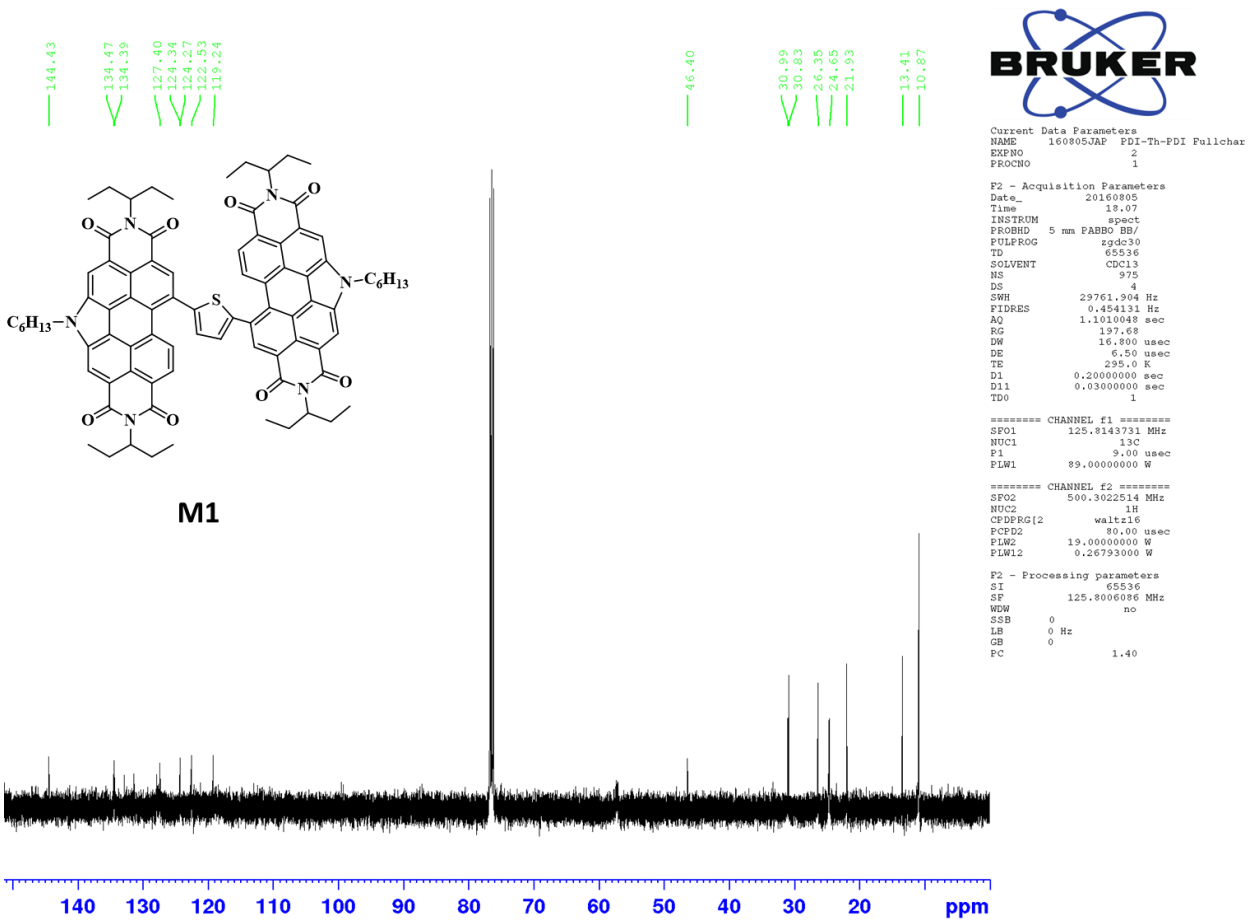

Figure S4: ^{13}C NMR spectrum of **M1**.

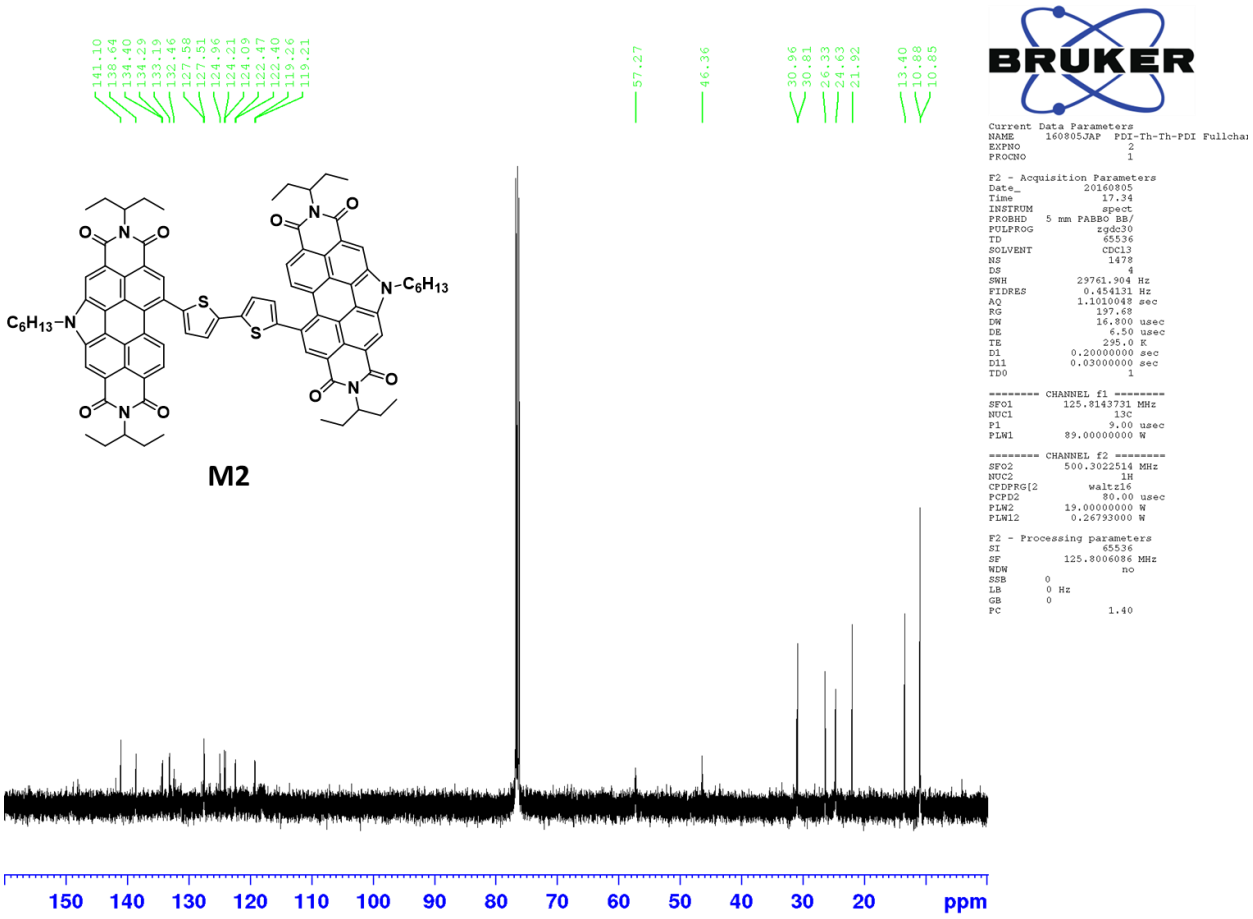

Figure S5: ^{13}C NMR spectrum of **M2**.

Mass Spectrometry:

-

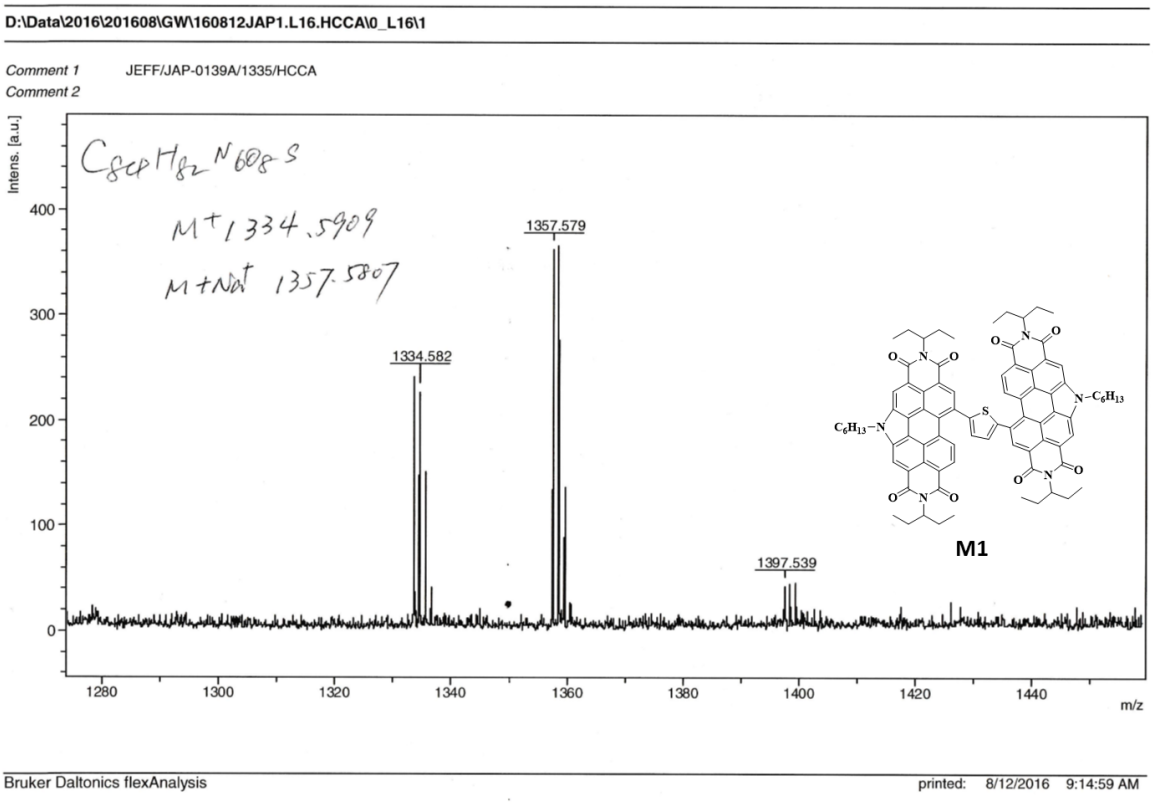

Figure S6: MALDI Spectrum of **M1** (molecular weight = 1335.67, M^+ = 1334.5909, $M+Na^+$ = 1357.5807).

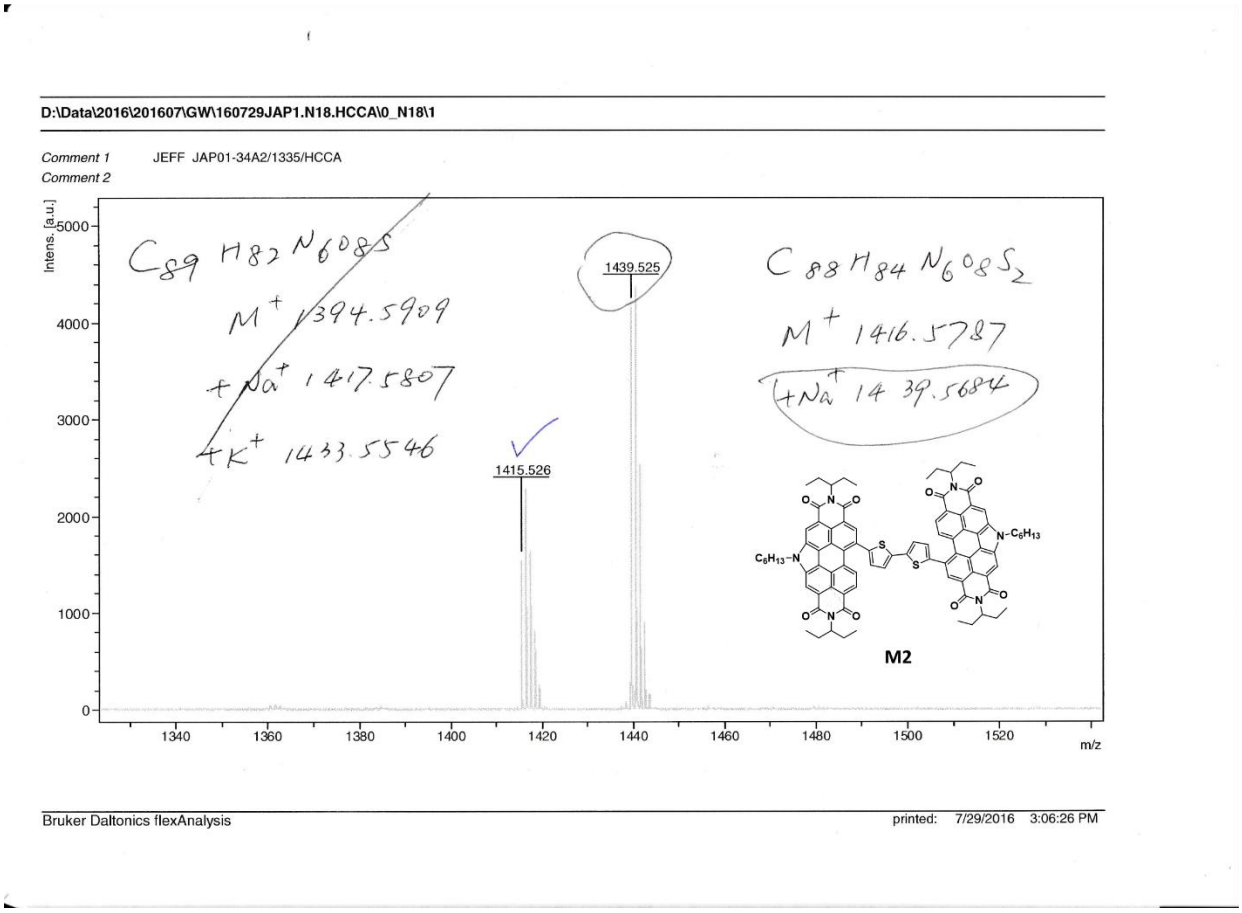

Figure S7: MALDI spectrum of **M2** (molecular weight = 1417.79, M^+ = 1416.5787, $M+Na^+$ = 1439.5684).

UV-Visible Spectroscopy: Calibration Curves:

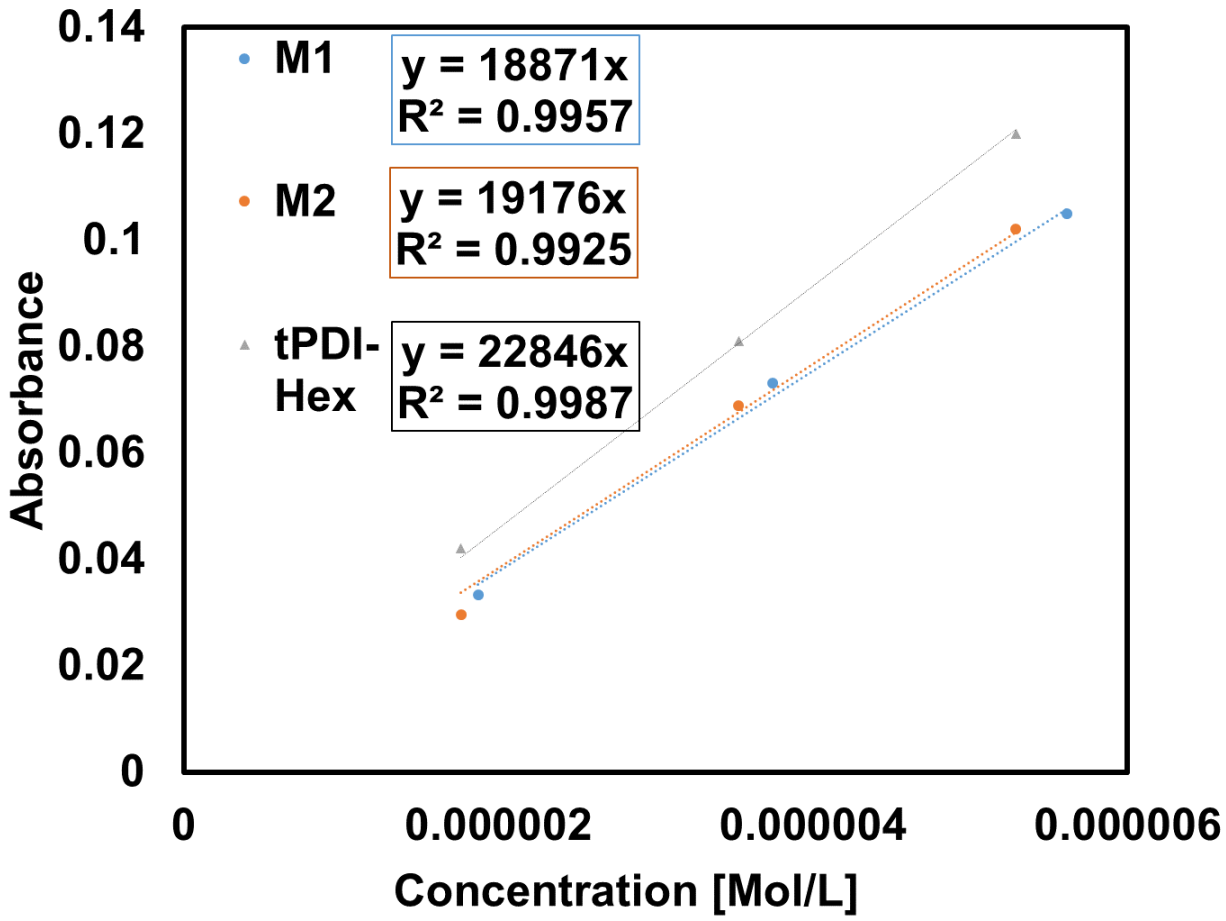

Figure S8: Absorbance vs. concentration plot used for the calculation of molar absorptivity. 0.2 cm path length was used for all measurements. Absorbance values were taken at λ_{max} for each compound.

Density Functional Theory:

Table S1: Summary of Predicted Optical Transitions

Molecule	State	E_{opt} (eV)	λ (nm)	f	Composition
tPDI-Hex	**S_3**	**2.52**	**492**	**0.587**	**H → L+1 (53%)**
		2.52	492	0.587	H-1 → L (44%)
	S_4	**2.54**	**488**	**0.496**	**H-1 → L+1 (52%)**
		2.54	488	0.496	H→L (45%)
	S_5	**2.81**	**442**	**0.228**	**H-2 → L (69%)**
		2.81	442	0.288	H-3→L+1 (26%)
M1	**S_4**	**2.51**	**494**	**0.936**	**H-1 → L+1 (43%)**
		2.51	494	0.936	H→L (23%)
		2.51	494	0.936	H-1→L (21%)
		2.51	494	0.936	H→L+1 (9%)
	S_5	**2.79**	**445**	**0.270**	**H-2→L+1 (53%)**
		2.79	445	0.270	H-3→L (39%)
M2	**S_1**	**2.19**	**565**	**0.155**	**H→L (80%)**
		2.19	565	0.155	H-1→L (19%)
	S_5	**2.54**	**488**	**0.371**	**H-2 → L (44%)**
		2.54	488	0.371	H-2→L+1 (25%)
		2.54	488	0.371	H-1→L+1 (10%)
		2.54	488	0.371	H→L (10%)
		2.54	488	0.371	H→L+1 (5%)
		2.54	488	0.371	H-1→L (5%)
	S_6	**2.56**	**484**	**0.589**	**H-2 → L+1 (40%)**
		2.56	484	0.589	H-1→L+1 (38%)
		2.56	484	0.589	H→L+1 (12%)

		2.56	484	0.589	H-2→L (6%)
	S_7	**2.82**	**439**	**0.180**	**H-4 → L (79%)**
		2.82	439	0.180	H-3→L+1 (11%)
		2.82	439	0.180	H-3→L (4%)
M2-90°	**S_5**	**2.54**	**489**	**0.213**	**H-2→L (60%)**
		2.54	489	0.213	**H→L (28%)**
		2.54	489	0.213	**H-1→L+1 (6%)**
		2.54	489	0.213	**H-2→L+1 (3%)**
	S_6	2.56	485	0.648	**H-1→L+1 (51%)**
		2.56	485	0.648	**H-2→L+1 (29%)**
	S_7	**2.81**	**441**	**0.200**	**H-3→L (85%)**
		2.81	441	0.200	H-4→L+1 (7%)
		2.81	441	0.200	H-4→L (2%)

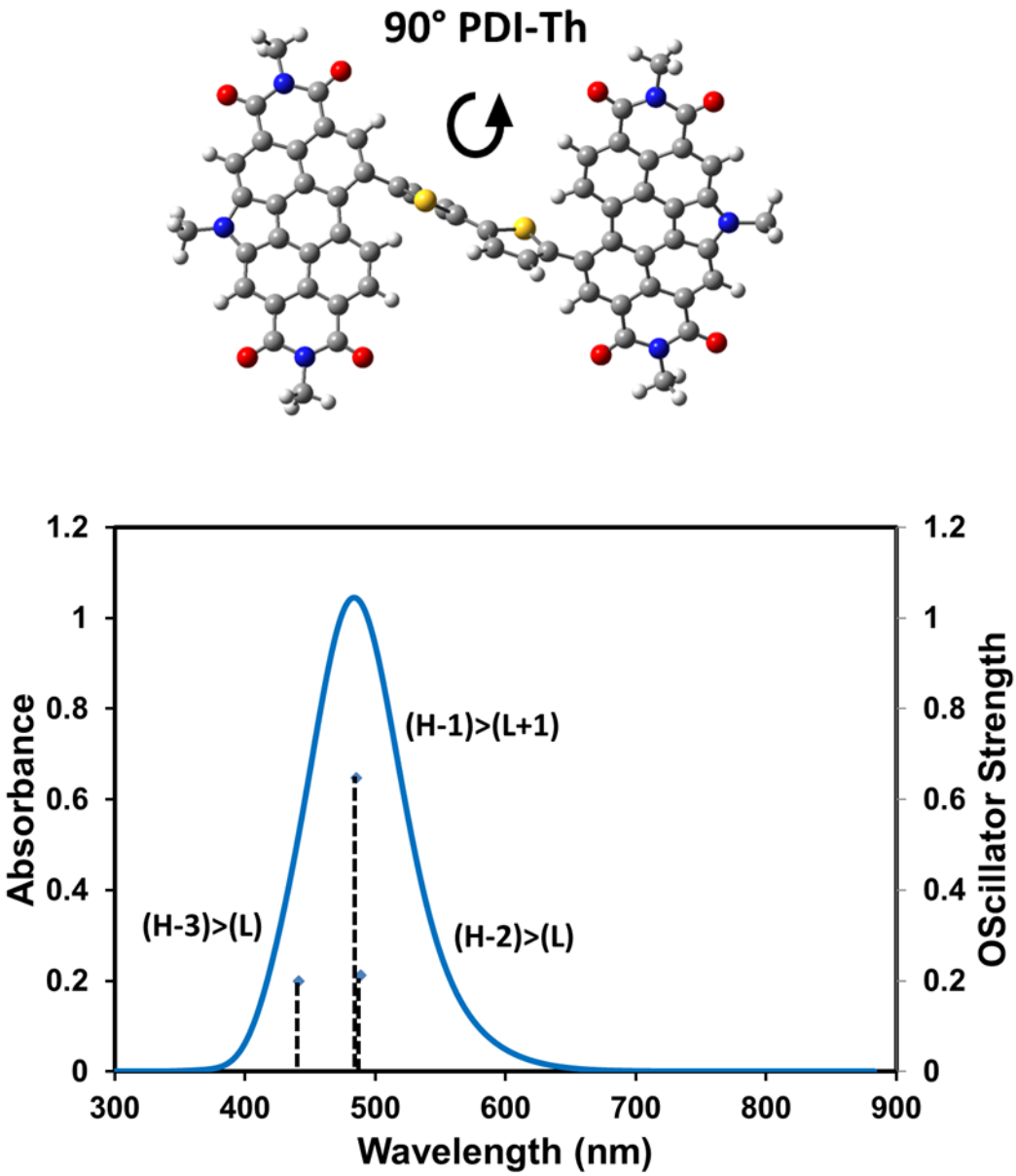

Figure S9: Calculated optical absorption profile for **M2**, with a 'locked' twist angle of 90 degrees between adjacent PDI and thiophene units. Calculations were done on Gaussian09,[2] input files and results were visualized using GausView05.[3] All alkyl chains were replaced with a methyl group. The B3LYP[4–6] level of theory with 6-31G(d,p)[7–12] basis set were used for the calculations. TD-SCF[13] calculations were performed from the optimized geometry, but with a modified PDI-Th dihedral angle of 90 degrees. The single point calculation was performed on this structure in order to generate molecular orbitals and electrostatic potential maps.

Polarized Optical Microscopy and X-Ray Diffraction:

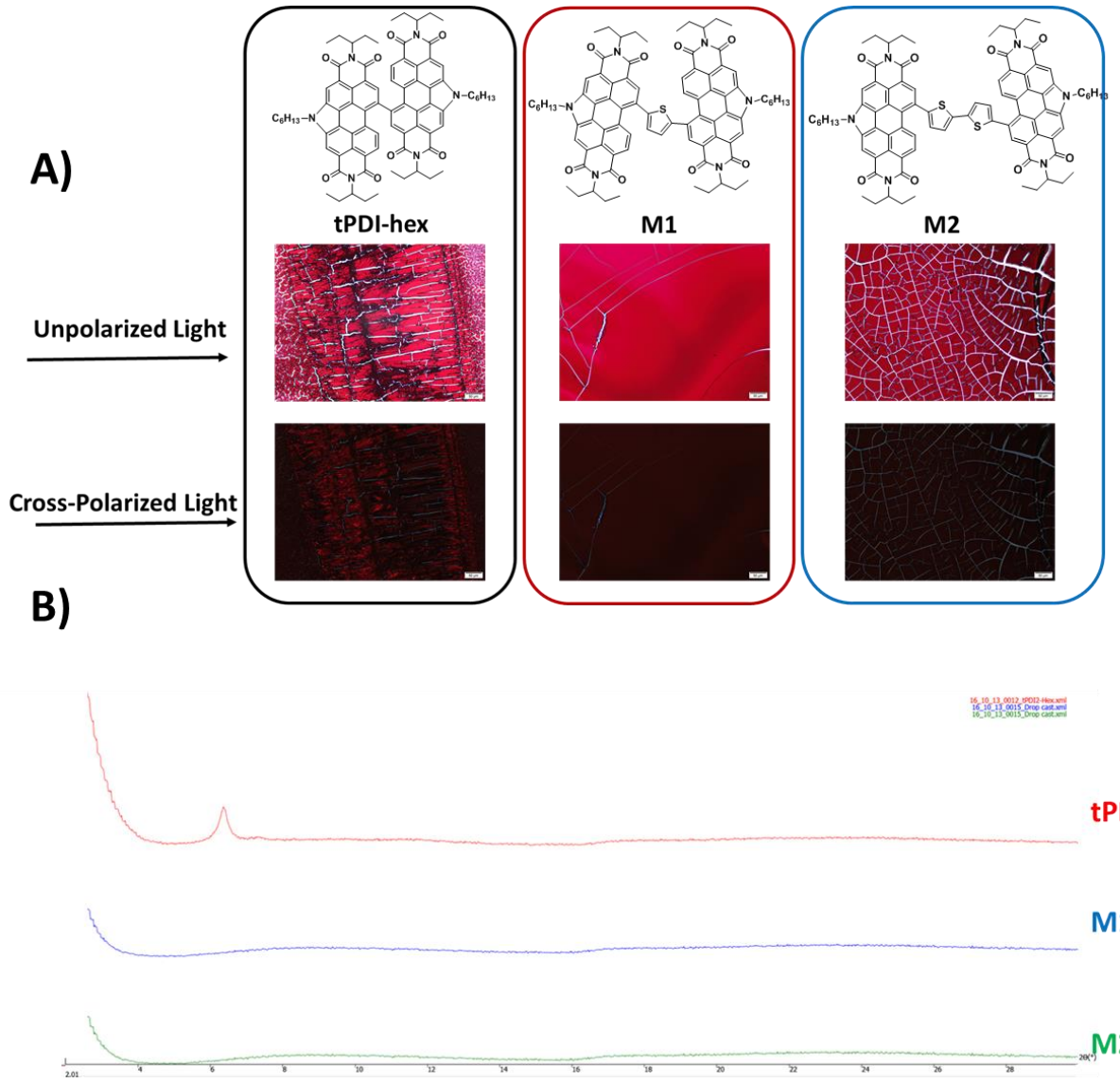

Figure S10: A) *top* - Optical microscopy study of drop cast films using unpolarized light. *Bottom*- Optical microscopy study of drop cast films using cross-polarized light. In each case the drop-cast films were made from a 20 mg/mL solution of the compound in chloroform. 20 µL was used to create each drop cast film. The enhanced crystallinity for **tPDI-hex** is clearly visible using polarized light images, while **M1** and **M2** appear to be non-crystalline. All images were taken at 20x magnification. **B)** X-ray diffraction patterns of drop cast films (Θ-2Θ scans), a peak at ~6.4 degrees is visible for **tPDI-Hex**, confirming the crystalline nature of the compound.

Photoluminescence Spectroscopy:

Photoluminescence experiments with the newly synthesized molecules revealed a trend of decreasing fluorescence intensity for molecules **tPDI-Hex**, **M1** and **M2** with increasing thiophene substitution. Previous reports by Müllen et al. noted a similar trend with decreasing fluorescence intensity of PDI based small molecules with increasing number of thiophenes connected in the α -positions.[16] Their studies, along with others have suggested that these type of PDI-thiophene molecules may experience photo-induced electron transfer (PET).[17–19] In order to confirm if this was occurring for **M1** and **M2**, we re-ran the emission spectra in a highly polar solvent, DMSO, which provides a thermodynamic driving force for the PET process between donor and acceptor moieties.[16] Upon re-running the emission spectra of **M1** and **M2** in DMSO, we noted a complete lack of emission intensity for these compounds, providing support for the assertion of a PET process between the electron rich thiophene units and electron poor PDI units of **M1** and **M2**. The parent dimer **tPDI-Hex** also showed a near complete quenching of the emission intensity in DMSO. This is likely not due to a photoinduced electron transfer process, as **tPDI-Hex** lacks the driving force for this, provided by the electron rich thiophene units in **M1** and **M2**. Studies have shown that decreased emission from highly symmetrical PDI oligomers can result from symmetry breaking charge transfer, resulting in decreased intensity for oligomeric PDI species compared to the parent monomers.[20] To examine this possibility, we performed the same photoluminescence experiment using a standard monomeric PDI molecule, namely N,N'-bis-ethylpropyl-perylene-3,4,9,10-tetracarboxylic-bisimide (EP2-PDI). This compound exhibited the highest emission intensity amongst the compounds studied (**Figure S11**), and only a slight decrease in intensity using DMSO as the solvent. This result reinforces the notation that intramolecular charge transfer processes are possible in the dimeric PDI compounds, however; further studies must be completed to unambiguously identify the origin of the observed fluorescence trends in our material series and to rule out other effects, such as rotational energy loss that could result in non-radiative decay for the excited species.

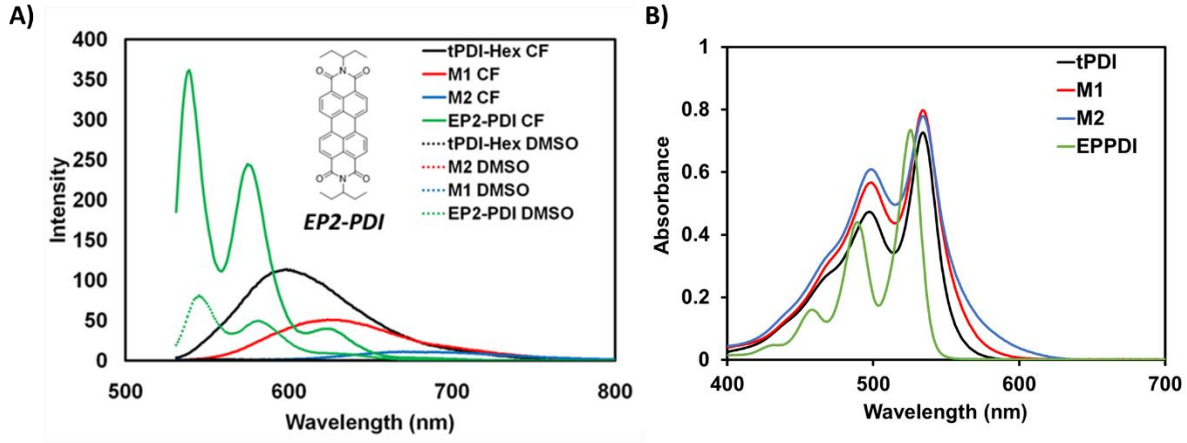

Figure S11: A) UV-Visible spectra, solutions of **tPDI-Hex**, **M1**, **M2,** and **EP2-PDI** in chloroform, solution concentrations were made so that the absorbance was approximately equal at λ_{max}. These solutions were then directly used for photoluminescence experiments. **B)** Photoluminescence spectra for compounds **tPDI-Hex**, **M1**, **M2,** and **EP2-PDI** in $CHCl_3$ and in DMSO solution. Compounds were excited at λ_{max} using 2.5 mm excitation and emission slit widths.

Solar Cell Devices:

Table S2: Summary of solar cell results from this work. Average values are from 4 devices.

Casting Solvent	Composition	Parameters	Voc (V)	Jsc (mA/cm^2)	FF(%)	PCE (%)
			Avg. (best) +/- stdev	Avg. (best) +/- stdev	Avg. (best) +/- stdev	Avg. (best) +/- stdev
CF	PTB7-Th:tPDI-Hex	2:3, as-cast	0.96 (0.96) +/- 0.02	11.59 (11.53) +/- 0.27	45.1 (47.3) +/- 1.76	5.0 (5.23) +/- 0.20
	PTB7-Th:tPDI-Hex	3:7, as-cast	0.96 (0.95) +/- 0.02	11.36 (11.49) +/- 0.11	44.3 (4.98) +/- 1.48	4.8 (5.0) +/- 0.13
	PTB7-Th:M1	2:3, as-cast	0.98 (0.93) +/- 0.06	3.67 (4.06) +/- 0.28	25.4 (26.4) +/- 1.25	0.9 (1.00) +/- 0.06
	PTB7-Th:M1	3:7, as-cast	0.93 (1.04) +/- 0.12	3.64 (4.08) +/- 0.35	26.5 (25.4) +/- 1.81	0.9 (1.08) +/- 0.12
	PTB7-Th:M2	2:3, as-cast	0.98 (0.97) +/- 0.05	4.21 (4.70) +/- 0.37	26.3 (27.6) +/- 1.16	1.1 (1.26) +/- 0.13
	PTB7-Th:M2	3:7, as-cast	1.05 (1.04) +/- 0.01	4.29 (4.49) +/- 0.25	25.7 (25.8) +/- 0.16	1.2 (1.21) +/- 0.07
O-Xyl.	PTB7-Th:tPDI-Hex	2:3 as-cast	0.93 (0.93) +/- 0.01	11.10 (10.88) +/- 0.58	45.6 (46.8) +/- 2.26	4.7 (4.73) +/- 0.03
	PTB7-Th:tPDI-Hex	3:7 as-cast	0.94 (0.95)) +/- 0.01	10.30 (10.41) +/- 0.53	48.8 (4.9) +/- 1.45	4.7 (4.82) +/- 0.15
	PTB7-Th:M1	2:3, as-cast	1.02 (1.05) +/- 0.03	5.45 (5.63) +/- 0.16	28.7 (28.1) +/- 1.10	1.6 (1.66) +/- 0.09
	PTB7-Th:M1	3:7, as-cast	0.98 (1.00) +/- 0.01	4.97 (5.59) +/- 0.62	30.7 (33.4) +/- 2.88	1.5 (1.86) +/- 0.35
	PTB7-Th:M2	2:3, as-cast	1.03 (1.02) +/- 0.01	6.67 (6.93) +/- 0.42	28.9 (29.6) +/- 1.01	2.0 (2.08) +/- 0.17
	PTB7-Th:M2	3:7, as-cast	1.05 (1.06) +/- 0.02	6.93 (6.90) +/- 0.12	29.7 (31.4) +/- 1.13	2.2 (2.30) +/- 0.10
	PTB7-Th:tPDI-Hex	3:7, as-cast	0.95 (0.95) +/- 0.01	10.03 (10.78) +/- 0.89	46.1 (44.6) +/- 2.37	4.4 (4.58) +/- 0.22
TMB	PTB7-Th:M1	3:7, as-cast	0.99 (0.99) +/- 0.01	5.53 (5.59) +/ 0.12	36.3 (36.7) +/- 0.79	2.0 (2.02) +/- 0.04
	PTB7-Th:M2	3:7, as-cast	1.05 (1.05) +/- 0.01	6.97 (7.17) +/- 0.20	36.2 (36.3) +/ 0.19	2.6 (2.74) +/- 0.09

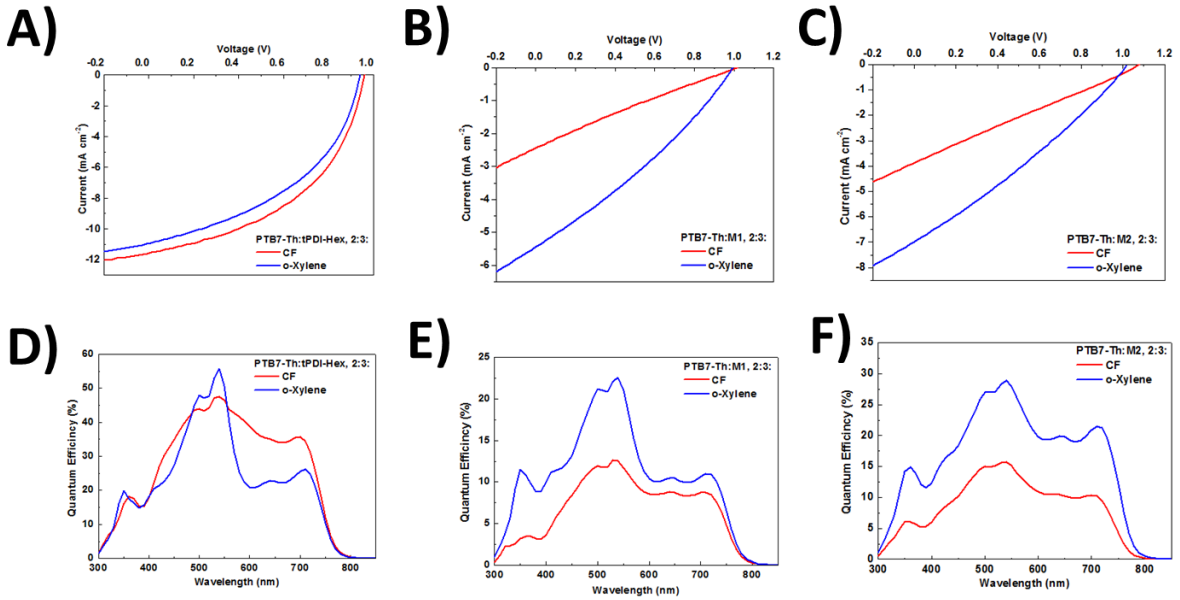

Figure S12: A) Current-Voltage curves of BHJ devices made using **tPDI-Hex** and **PTB7-Th**. **B)** Incident photon to current efficiency (IPCE, EQE) of BHJ devices made using **tPDI-Hex** and **PTB7-Th**. **C)** Current-Voltage curves of BHJ devices made using **M1** and **PTB7-Th**. **D)** Incident photon to current efficiency (IPCE, EQE) of BHJ devices made using **M1** and **PTB7-Th**. **E)** Current-Voltage curves of BHJ devices made using **M2** and **PTB7-Th**. **F)** Incident photon to current efficiency (IPCE, EQE) of BHJ devices made using **M2** and **PTB7-Th**. All data shown is from devices using a 2:3 Donor:Acceptor ratio.

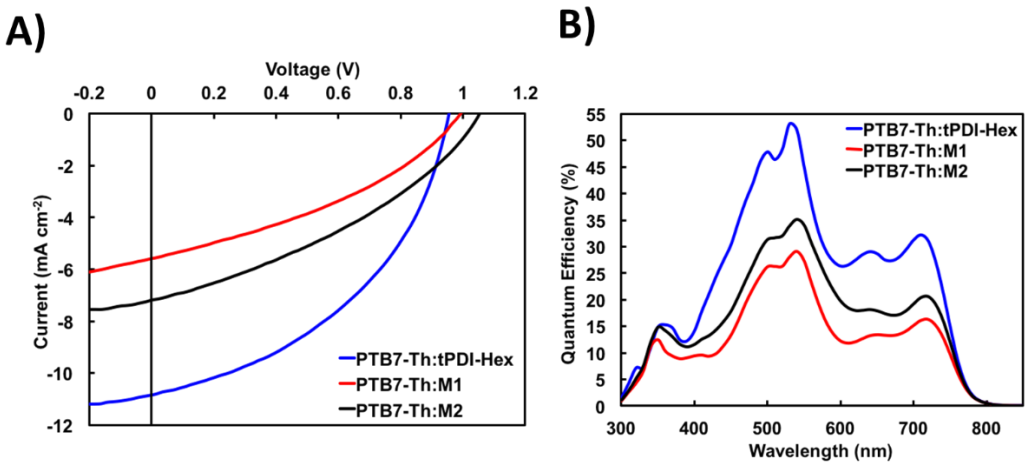

Figure S13: A) Current-Voltage curves of BHJ devices made using **M1**, **M2** and **tPDI-Hex** acceptors and **PTB7-Th** as the donor. The casting solvent was TMB. **B)** Incident photon to current efficiency (IPCE, EQE) of BHJ devices made using **M1**, **M2** and **tPDI-Hex** acceptors and **PTB7-Th** as the donor All data shown is from inverted devices using a 3:7 Donor:Acceptor ratio.

Photoluminescence Quenching:

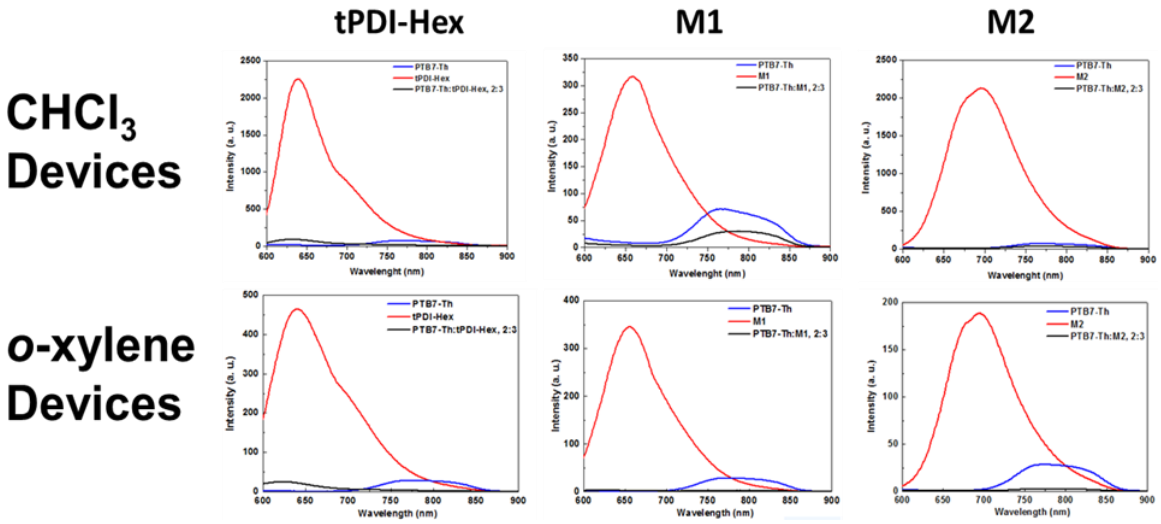

Figure S14: Photoluminescence spectra of the blend heterojunction films cast at a **2:3** Donor:acceptor ratio and excited at 530 nm, using 5 mm and 10 mm excitation and emission slit widths, respectively.

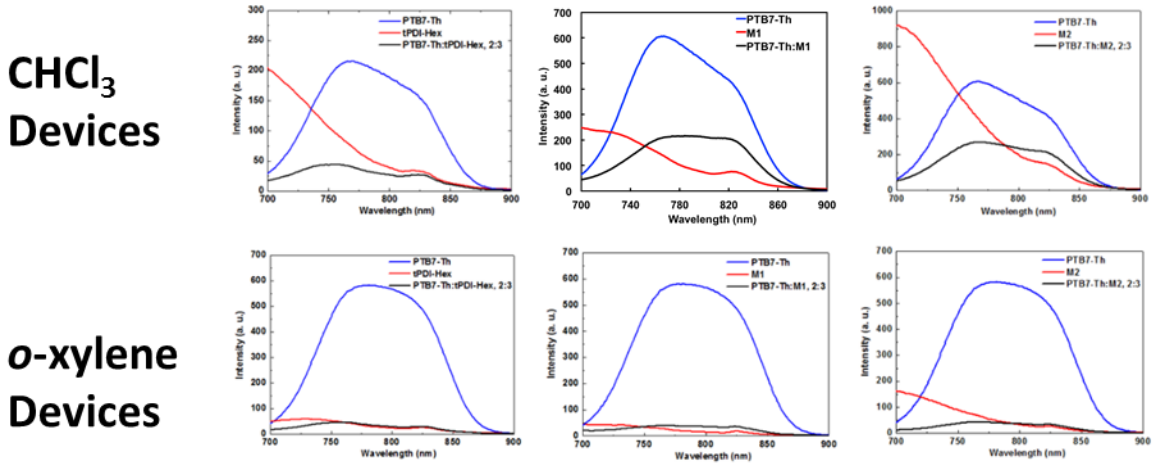

Figure S15: Photoluminescence spectra of the blend heterojunction films cast at a **2:3** Donor:acceptor ratio and excited at 640 nm, using 5 mm and 10 mm excitation and emission slit widths, respectively.

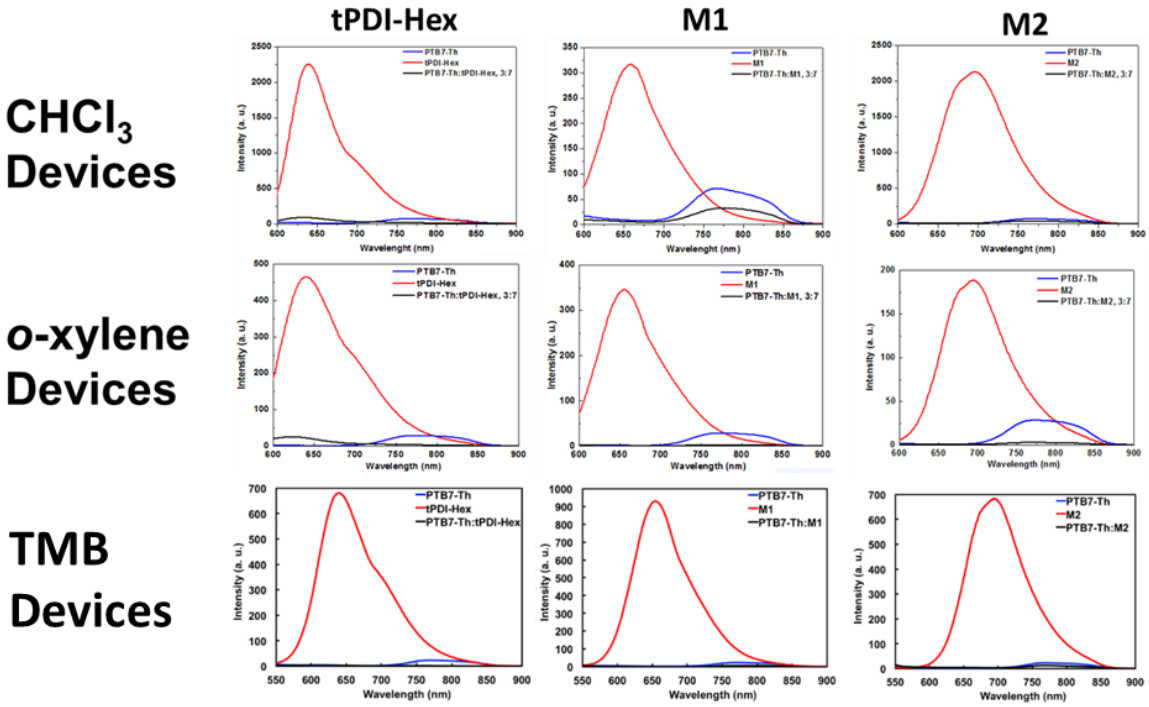

Figure S16: Photoluminescence spectra of the blend heterojunction films cast at a **3:7** Donor:acceptor ratio and excited at 530 nm, using 5 mm and 10 mm excitation and emission slit widths, respectively.

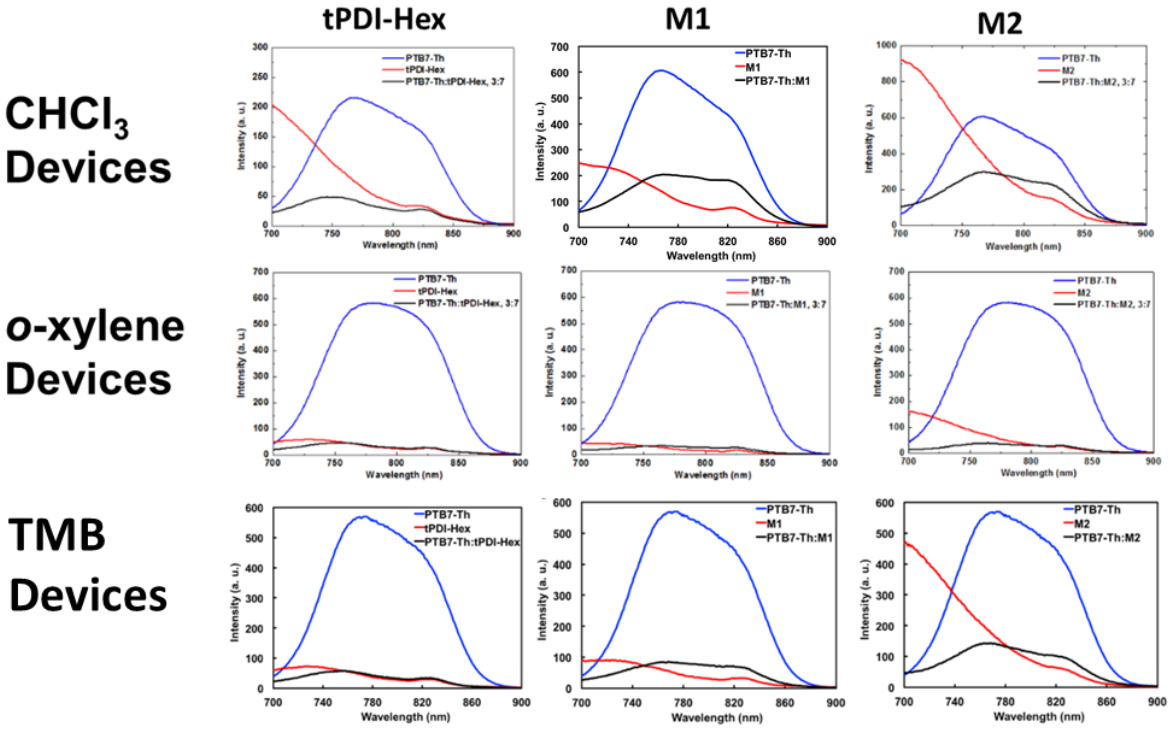

Figure S17: Photoluminescence spectra of the blend heterojunction films cast at a **3:7** Donor:acceptor ratio and excited at 640 nm, using 5 mm and 10 mm excitation and emission slit widths, respectively.

Atomic Force Microscopy:

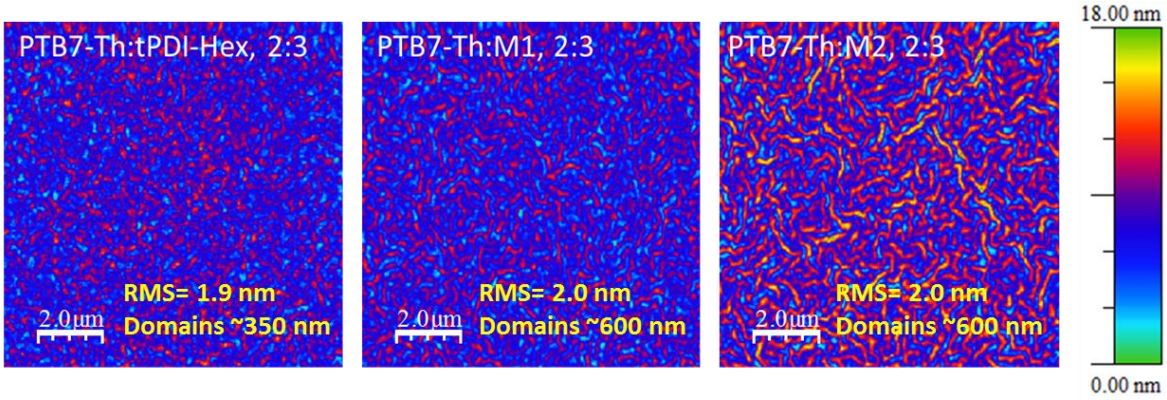

Figure S18: Contact AFM surface scans (size: 10x10μm) of the BHJ films cast from **chloroform** at a 2:3 Donor:Acceptor ratio. Measurements made on solar cell devices in-between the Ag contacts.

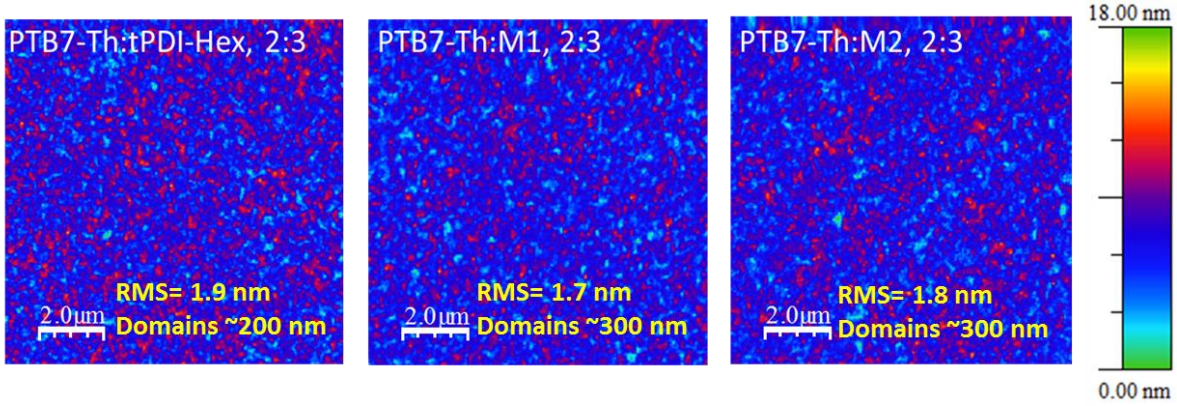

Figure S19: Contact AFM surface scans (size: 10x10μm) of the BHJ films cast from ***o*-xylene** at a 2:3 Donor:Acceptor ratio. Measurements made on solar cell devices in-between the Ag contacts.

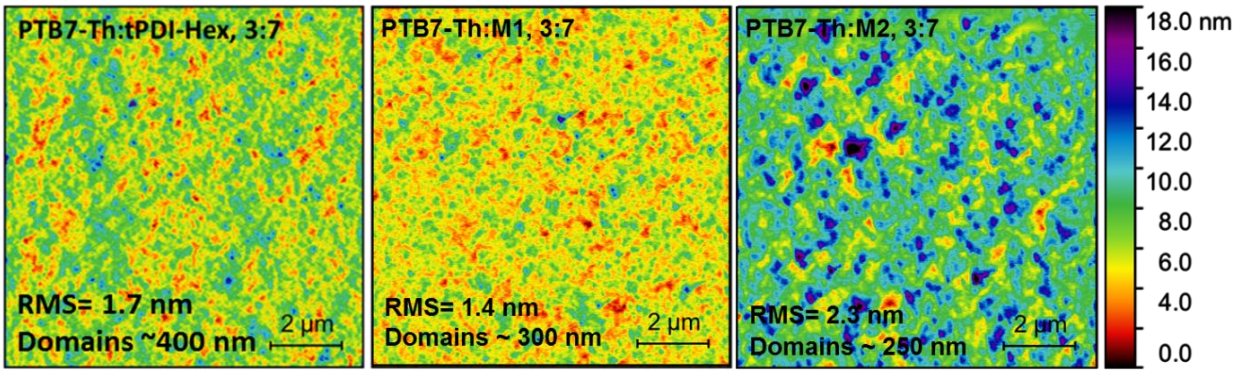

Figure S20: Non-contact (tapping mode) AFM surface scans (size: 10x10μm) of the BHJ films cast from **TMB** at a 3:7 Donor:Acceptor ratio. Measurements made on solar cell devices in-between the Ag contacts.

References:

(1) Hendsbee, A. D.; Sun, J.-P.; Law, W. K.; Yan, H.; Hill, I. G.; Spasyuk, D. M.; Welch, G. C. *Chem. Mater.* **2016**, *28* (19), 7098–7109.
(2) Frisch, M.; Trucks, G.; Schlegel, H.; Scuseria, G.; Robb, M.; Cheeseman, J.; Scalmani, G.; Barone, V.; Mennucci, B.; Petersson, G.; Nakatsuji, H.; Caricato, M.; Li, X.; Hratchian, H.; Izmaylov, A.; Bloino, J.; Zheng, G.; Sonnenberg, J.; Hada, M.; Ehara, M.; Toyota, K.; Fukuda, R.; Hasegawa, J.; Ishida, M.; Nakajima, T.; Honda, Y.; Kitao, O.; Nakai, H.; Vreven, T.; Montgomery, J.; Peralta, J.; Ogliaro, F.; Bearpark, M.; Heyd, J.; Brothers, E.; Kudin, K.; Staroverov, V.; Kobayashi, R.; Normand, J.; Raghavachari, K.; Rendell, A.; Burant, J.; Iyengar, S.; Tomasi, J.; Cossi, M.; Rega, N.; Millam, J.; Klene, M.; Knox, J.; Cross, J.; Bakken, V.; Adamo, C.; Jaramillo, J.; Gomperts, R.; Stratmann, R.; Yazyev, O.; Austin, A.; Cammi, R.; Pomelli, C.; Ochterski, J.; Martin, R.; Morokuma, K.; Zakrzewski, V.; Voth, G.; Salvador, P.; Dannenberg, J.; Dapprich, S.; Daniels, A.; Farkas; Foresman, J.; Ortiz, J.; Cioslowski, J.; Fox, D. *Gaussian 09 Revis. B01 Gaussian Inc Wallingford CT* **2009**.
(3) *GaussView Version 5*.
(4) Becke, A. D. *Phys. Rev. A* **1988**, *38* (6), 3098–3100.
(5) Lee, C.; Yang, W.; Parr, R. G. *Phys. Rev. B* **1988**, *37* (2), 785–789.
(6) Miehlich, B.; Savin, A.; Stoll, H.; Preuss, H. *Chem. Phys. Lett.* **1989**, *157* (3), 200–206.
(7) Hehre, W. J.; Ditchfield, R.; Pople, J. A. *J. Chem. Phys.* **1972**, *56* (5), 2257–2261.
(8) Hariharan, P. C.; Pople, J. A. *Theor. Chim. Acta* **1973**, *28* (3), 213–222.
(9) Francl, M. M.; Pietro, W. J.; Hehre, W. J.; Binkley, J. S.; Gordon, M. S.; DeFrees, D. J.; Pople, J. A. *J. Chem. Phys.* **1982**, *77* (7), 3654–3665.
(10) Binning, R. C.; Curtiss, L. A. *J. Comput. Chem.* **1990**, *11* (10), 1206–1216.
(11) Rassolov, V. A.; Pople, J. A.; Ratner, M. A.; Windus, T. L. *J. Chem. Phys.* **1998**, *109* (4), 1223–1229.
(12) Rassolov, V. A.; Ratner, M. A.; Pople, J. A.; Redfern, P. C.; Curtiss, L. A. *J. Comput. Chem.* **2001**, *22* (9), 976–984.
(13) Bauernschmitt, R.; Ahlrichs, R. *Chem. Phys. Lett.* **1996**, *256* (4–5), 454–464.
(14) Sun, Y.; Seo, J. H.; Takacs, C. J.; Seifter, J.; Heeger, A. J. *Adv. Mater.* **2011**, *23* (14), 1679–1683.
(15) Kuo, C.-Y.; Huang, Y.-C.; Hsiow, C.-Y.; Yang, Y.-W.; Huang, C.-I.; Rwei, S.-P.; Wang, H.-L.; Wang, L. *Macromolecules* **2013**, *46* (15), 5985–5997.
(16) Wonneberger, H.; Ma, C.-Q.; Gatys, M. A.; Li, C.; Bäuerle, P.; Müllen, K. *J. Phys. Chem. B* **2010**, *114* (45), 14343–14347.
(17) Balaji, G.; Kale, T. S.; Keerthi, A.; Della Pelle, A. M.; Thayumanavan, S.; Valiyaveettil, S. *Org. Lett.* **2011**, *13* (1), 18–21.
(18) Huang, J.; Wu, Y.; Fu, H.; Zhan, X.; Yao, J.; Barlow, S.; Marder, S. R. *J. Phys. Chem. A* **2009**, *113* (17), 5039–5046.
(19) Chen, S.; Liu, Y.; Qiu, W.; Sun, X.; Ma, Y.; Zhu, D. *Chem. Mater.* **2005**, *17* (8), 2208–2215.
(20) Wu, Y.; Young, R. M.; Frasconi, M.; Schneebeli, S. T.; Spenst, P.; Gardner, D. M.; Brown, K. E.; Würthner, F.; Stoddart, J. F.; Wasielewski, M. R. *J. Am. Chem. Soc.* **2015**, *137* (41), 13236–13239.